Metal–Organic Layers Hot Paper

Deutsche Ausgabe: DOI: 10.1002/ange.201512054
Internationale Ausgabe: DOI: 10.1002/anie.201512054

Self-Supporting Metal–Organic Layers as Single-Site Solid Catalysts

Lingyun Cao[+], Zekai Lin[+], Fei Peng[+], Weiwei Wang, Ruiyun Huang, Cheng Wang, Jiawei Yan, Jie Liang, Zhiming Zhang, Teng Zhang, Lasheng Long, Junliang Sun,* and Wenbin Lin**

Abstract: *Metal–organic layers (MOLs) represent an emerging class of tunable and functionalizable two-dimensional materials. In this work, the scalable solvothermal synthesis of self-supporting MOLs composed of $[Hf_6O_4(OH)_4(HCO_2)_6]$ secondary building units (SBUs) and benzene-1,3,5-tribenzoate (BTB) bridging ligands is reported. The MOL structures were directly imaged by TEM and AFM, and doped with 4′-(4-benzoate)-(2,2′,2″-terpyridine)-5,5″-dicarboxylate (TPY) before being coordinated with iron centers to afford highly active and reusable single-site solid catalysts for the hydrosilylation of terminal olefins. MOL-based heterogeneous catalysts are free from the diffusional constraints placed on all known porous solid catalysts, including metal–organic frameworks. This work uncovers an entirely new strategy for designing single-site solid catalysts and opens the door to a new class of two-dimensional coordination materials with molecular functionalities.*

As the majority of industrially used catalysts are heterogeneous, it is desirable to immobilize molecular catalysts onto porous solid supports that are compatible with industrial processes. Metal–organic frameworks (MOFs), porous solids that are assembled from organic ligands and metal coordination nodes, have provided a versatile platform for the heterogenization of molecular catalysts.[1] However, their activity is often limited by the rates of diffusion of substrates and products within the frameworks.[2] This diffusional constraint can be relieved by reducing one dimension of the MOF crystal to only a few nanometers to minimize the diffusion distance. This dimensional reduction results in two-dimensional (2D) metal–organic layers (MOLs), a new category of 2D materials. MOLs not only provide the benefit of readily accessible active sites in a thin layer but also inherit the heterogeneous nature, ordered structure, and molecular tunability of MOF catalysts.

2D coordination layers have been reported in the literature,[3] along with other prominent 2D materials, such as graphenes and metal dichalcogenides.[4] 2D coordination layers were previously assembled on flat metal surfaces[5] or created at air/liquid or liquid/liquid interfaces by the Langmuir–Blodgett method.[6] However, these methods cannot produce sufficient quantities of self-supporting nanosheets for catalytic applications. Recently, top-down chemical or physical exfoliation has also been used to prepare nanosheets from layered 3D MOFs.[7] Herein, we report a highly scalable bottom-up strategy to assemble MOLs directly from molecular building blocks in one-pot solvothermal reactions. Importantly, the MOLs were functionalized with Fe catalytic centers to give diffusion-free heterogeneous catalysts.

Nanostructures with a high surface energy, such as MOLs, can in principle be prepared in the presence of surfactants, which reduce the surface energy through the hydrophobic protecting shell but also block the catalytic sites.[8] Alternatively, nanoparticles with high index facets (with high surface energies) can be prepared by crystallization under supersaturation conditions.[9] This strategy can be rationalized by the Thomson–Gibbs equation,

$$\Delta\mu = \mu_l - \mu_c = \sigma S \quad (1)$$

which relates the difference between the chemical potentials ($\Delta\mu$) of the species in the supersaturated solution (μ_l) and the crystallized ones (μ_c) to additional surface energies of the crystallites (σS) as a result of energy conservation. We combined the above two strategies to create MOLs by 1) introducing small capping molecules that reduce the surface energy penalty without blocking the catalytic sites and 2) creating a supersaturation of the building blocks in the solution for MOL synthesis to tolerate additional surface energies as compared to the bulk 3D crystals.

The Hf^{4+} cluster $[Hf_6(\mu_3\text{-}O)_4(\mu_3\text{-}OH)_4(carboxylate)_{12}]$[10] was chosen for the MOL synthesis because of the tendency of Hf to form stable coordination bonds with carboxylates. The 12-connectivity of the Hf_6 cluster, however, violates the geometric requirement of a 2D layer. We used a capping method to overcome the geometric mismatch. In this method, six of the connection sites on the cluster were protected by formate groups, leaving the remaining six in the same plane to connect to the benzene-1,3,5-tribenzoate (BTB) moieties. The 6-connected Hf_6 secondary building units (SBUs) and the three-connected BTB ligands link to each other to form an

[*] L. Cao,[+] W. Wang, R. Huang, Prof. C. Wang, Prof. J. Yan, Prof. Z. Zhang, Prof. L. Long, Prof. W. Lin
College of Chemistry and Chemical Engineering, iCHEM, PCOSS
Xiamen University, Xiamen 361005 (China)
E-mail: wangchengxmu@xmu.edu.cn
Z. Lin,[+] T. Zhang, Prof. W. Lin
Department of Chemistry, University of Chicago
Chicago, IL 60637 (USA)
E-mail: wenbinlin@uchicago.edu
F. Peng,[+] J. Liang, Prof. J. Sun
Berzelii Center EXCELLENT on Porous Materials
Department of Materials and Environmental Chemistry
Stockholm University, 10691 Stockholm (Sweden)
Prof. J. Sun
College of Chemistry and Molecular Engineering
Peking University, 100871 Beijing (China)
E-mail: junliang.sun@pku.edu.cn
[+] These authors contributed equally to this work.
Supporting information and the ORCID identification number(s) for the author(s) of this article can be found under http://dx.doi.org/10.1002/anie.201512054.

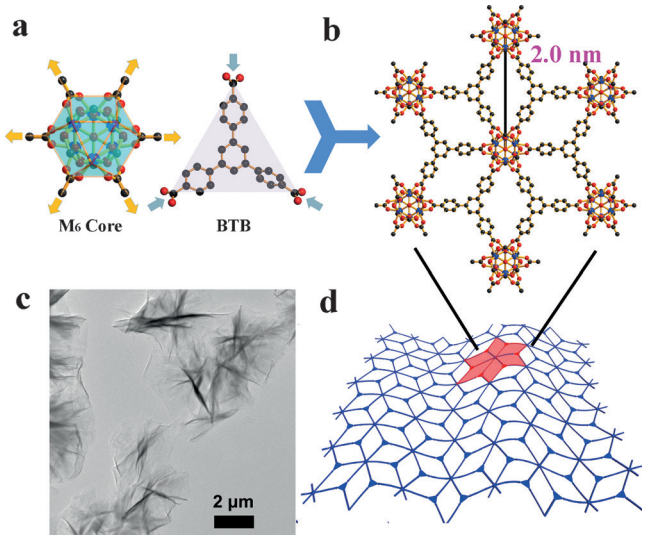

Figure 1. a) The $[Hf_6O_4(OH)_4(HCO_2)_6(carboxylate)_6]$ SBU in MOLs with the connectivity indicated by golden arrows; structure of the BTB ligand with the connectivity indicated by light blue arrows. b) Formation of the 2D kgd lattice from 6-connected SBUs and 3-connected BTB ligands. C black, Hf blue, O red. c) TEM image of $Hf_6O_4(OH)_4(HCO_2)_6(BTB)_3$ nanosheets. d) Structural representation of the ruffled sheet with kgd topology.

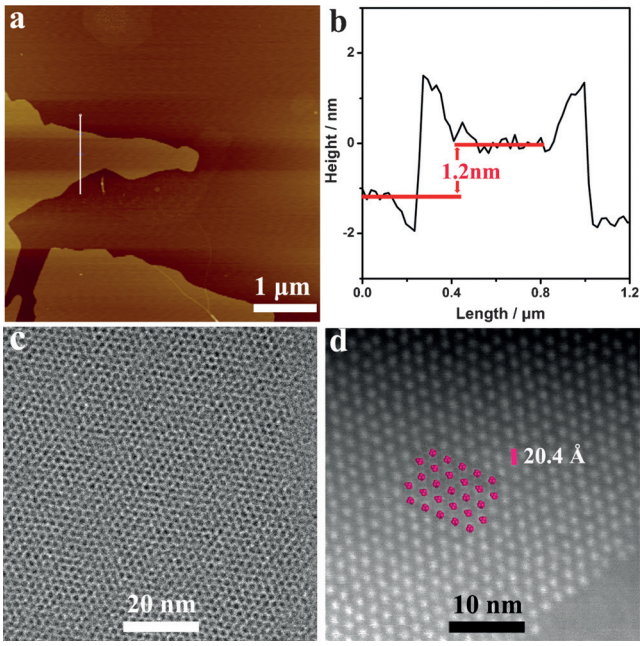

Figure 2. a) Tapping-mode AFM topography. b) The height profile along the white line in (a). c) HRTEM image of the MOL. d) HAADF image of the MOL.

infinite 3,6-connected 2D network of $Hf_6(\mu_3\text{-}O)_4(\mu_3\text{-}OH)_4(HCO_2)_6(BTB)_2$ with kagome dual (kgd) topology (Figure 1). The supersaturation of the SBU in the crystallization solution was created by adding water to the reaction mixture to take advantage of the partial hydrolysis of Hf^{4+}: $6\,Hf^{4+} + 8\,H_2O + 6\,HCO_2H \rightarrow [Hf_6(\mu_3\text{-}O)_4(\mu_3\text{-}OH)_4(HCO_2)_6]^{6+} + 18\,H^+$. Furthermore, water also accelerates *N*,*N*-dimethylformamide (DMF) decomposition to generate dimethylamine, which neutralizes the HCl generated during the reaction. Uniform MOLs down to monolayer thickness can be obtained using a reactant molar ratio of $HfCl_4/BTB/HCO_2H/H_2O/DMF = 1.5:1:830:290:2280$ by heating the mixture at 120 °C for 48 hours.

Transmission electron microscopy (TEM) images showed the MOLs to be wrinkled ultrathin films with an average sheet area of approximately $4 \times 4\ \mu m^2$ (Figure 1c). The as-prepared MOLs were highly creased to minimize surface energy, resembling images of other 2D materials, such as reduced graphene oxide (rGO).[11] The powder X-ray diffraction (PXRD) patterns of the sample give only three broad intralayer peaks, which is consistent with our pattern modelled for MOLs with one or two layers (Supporting Information, Figure S7). These nanofilms also exhibit a high specific surface area of 661.7 $m^2 g^{-1}$ according to nitrogen adsorption measurements (Figure S10). The surface area of MOL monolayers was simulated to be 883 $m^2 g^{-1}$ by using the Materials Studio software.

Atomic force microscopy (AFM) images of the MOLs gave monolayer thickness for many of the nanosheets. The measured height of 1.2 ± 0.2 nm (Figure 2) is very close to the van der Waals size of the Hf_6 cluster. The edges of the measured monolayers were usually slightly higher than the middle part because of the wrinkling. Nanosheets with a thickness of 2.2 ± 0.2 nm and 3.2 ± 0.2 nm were also found (Figure S3), and correspond to bilayer and trilayer structures.

The chemical structures of the monolayer and stacked multilayers were analyzed by high-resolution transmission electron microscopy (HRTEM) and scanning transmission electron microscopy (STEM). The direct imaging of MOF lattices has only been reported a few times.[12] The HRTEM images of the MOLs showed clear lattice fringes. The Hf_6 clusters appear as dark spots on the images as compared to the background and non-metallic atoms, which is consistent with a positive contrast (Figure 2c). In the high-angle annular dark field (HAADF) images taken in STEM mode, clear 2D kgd nets with white spots representing the Hf_6 clusters were observed (Figure 2d). The arrangement of the spots matches our proposed atomic model of the kgd monolayer. The distances between adjacent spots in the HRTEM image (20.1 Å) and the STEM-HAADF image (20.4 Å) match that between two adjacent SBUs in the atomic model (20.02 Å). Aside from the regular kgd lattice, we also observed a number of distorted lattices or complex lines and even ripples in the HRTEM/STEM-HAADF images. These features were either due to tilted sample orientations or stacked layers with a Moiré pattern (Figure S4).

A 3D reciprocal lattice was reconstructed from the rotation electron diffraction (RED) data of the MOLs (Figure 3). The spots in the reciprocal space showed a hexagonal pattern along the c^* axis perpendicular to the thin layer, which is consistent with the 2D kgd net (Figure 3a). This lattice could be indexed to a hexagonal unit cell with $a = 19.4$ Å, which corresponds well to our model within the experimental error. In directions parallel to the layers, streaks of diffraction rods were observed (Figure 3b,c), which are characteristic of very thin films. These patterns match our simulations of the monolayer (Figure S6.3).

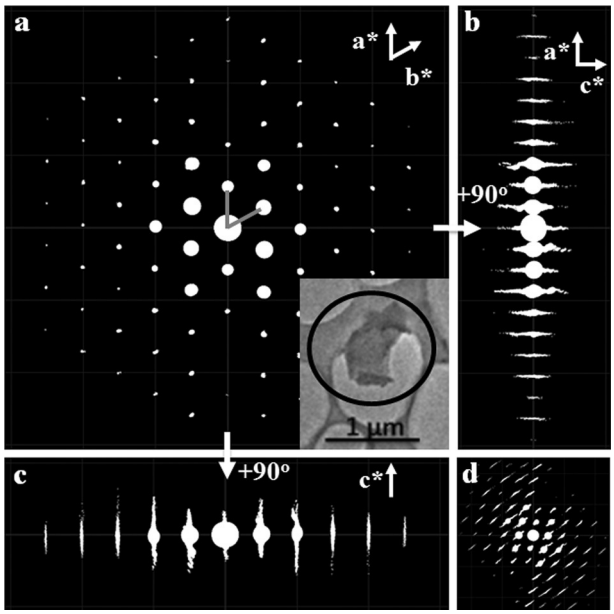

Figure 3. Reconstructed 3D reciprocal lattice from the RED data. a) The reciprocal lattice along *c**, perpendicular to the nanosheet. b) The reciprocal lattice obtained from rotating (a) by 90° with respect to the vertical axis. c) The reciprocal lattice obtained from rotating (a) by 90° with respect to the horizontal axis. d) One representative image of the 3D RED data. The inset in (a) is the TEM image of the selected nanosheet.

Consistent with our proposed structural model, we observed such layers in the X-ray structures of two closely related 3D single crystals.[13] Single crystals of a MOF with the framework formula $Zr_6(\mu_3\text{-}O)_4(\mu_3\text{-}OH)_4(HCO_2)_6(BTB)_2$ (Zr-MOF1; see Figure S8c) were obtained by us and others[10b] using $ZrOCl_2{\cdot}8H_2O$ as the metal source. The same crystalline phase for Hf was also obtained (Hf-MOF1; see Figure S2.2 for the PXRD patterns). Zr-MOF1 contains the aforementioned 3,6-connected kgd layers (Figure 1b), which are interlocked within each other in two orthogonal directions to give the 3D structure. Six formates act as the capping ligands for six (out of twelve) connections on the Zr_6 SBUs. In another crystal structure (Zr-MOF2 and Hf-MOF2) with the same framework formula, the same 2D kgd layers are stacked on each other in a staggered arrangement (Figure S8b). The observation of such layers as building blocks of the 3D crystal structures confirms the feasibility of our proposed MOL atomic model.

X-ray absorption spectroscopy was used to further characterize the Hf_6 SBU in the MOLs. The Fourier-transformed EXAFS profiles of the MOLs were very similar to those of Hf-MOF1, confirming a common SBU for the two structures. EXAFS fitting showed that the Hf^{4+} ions are coordinated by eight oxygen atoms in the SBU, with Hf–(μ_3-O) distances of 2.26 ± 0.01 Å, Hf–(μ_3-OH) distances of 2.30 ± 0.01 Å, and Hf–O(carboxylate) distances of 2.12 ± 0.01 Å (Figure S13). We ascertained and quantified the formate capping ligands by EXAFS and NMR spectroscopy. First, fitting the EXAFS data to the secondary sphere of Hf^{4+} gives Hf–C(BTB) distances of 3.15 ± 0.03 Å and Hf–C(formate) distances of 3.22 ± 0.03 Å, which corresponds to six formates as the capping groups and six carboxylates from the BTB ligands. Second, the ^{1}H NMR spectrum of the digested MOLs gives a molar ratio of formate/BTB = 3:1 (Figure S5), which matches the one expected from the formate-capped structure.

The MOLs were then doped with the ligand 4′-(4-benzoate)-(2,2′,2″-terpyridine)-5,5″-dicarboxylate (TPY) by taking advantage of the matching shape and size between TPY and BTB (Figure 4). The resultant TPY-MOL with 30% TPY (based on the total number of tridentate ligands) was metalated with $FeBr_2$ (1.05 equiv relative to TPY) and activated by $NaBHEt_3$. The final Fe-TPY-MOL catalyst contains 100% of Fe with respect to TPY as determined by ICP-MS. PXRD (Figure S14) and TEM (Figure 4) studies confirmed that the Fe-TPY-MOL catalyst adopts the same nanosheet structure as the undoped MOL. As control samples, the 3D interlocked Hf-MOF1 and 3D stacked Hf-MOF2 were also doped with the TPY ligand (Figure S9.2.2 and S9.2.3), metalated with $FeBr_2$, and treated with $NaBHEt_3$ to give Fe-TPY-MOF1 and Fe-TPY-MOF2. A homogeneous control sample was prepared by mixing equal amounts of TPY and $FeBr_2$ in THF, followed by reduction with $NaBHEt_3$.

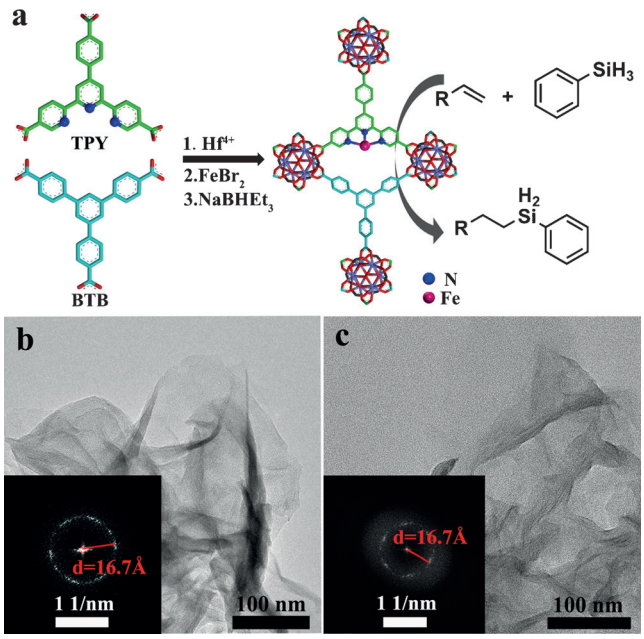

Figure 4. a) Preparation of the MOL catalyst Fe-TPY-MOL. b,c) HRTEM and FFT images of Fe-TPY-MOL before (b) and after catalysis (c).

We rationalized that MOLs might provide a sterically protective environment to endow TPY-Fe catalytic activity in the hydrosilylation of olefins.[14] At a catalyst loading of 0.02%, Fe-TPY-MOL catalyzed the hydrosilylation of styrene to afford the pure anti-Markovnikov product in complete conversion over 48 hours (Table 1, entry 1), which corresponds to a turnover number (TON) of > 5000. In contrast, no conversion was observed for the MOF with an interlocked 3D structure, Fe-TPY-MOF1 (Table 1, entry 2), and only 30% product was obtained for the Fe-TPY-MOF2 with a stacked

Table 1: MOLs loaded with Fe catalytic centers for the hydrosilylation of terminal olefins.

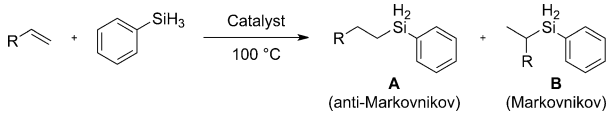

Entry	Olefin	Cat. (mol%)	*t*	Yield [%] A/B[a]
1		Fe-TPY-MOLs (0.02)	2 d	100/0
2		Fe-TPY-MOF1 (0.02)	6 d	0
3		Fe-TPY-MOF2 (0.02)	2 d	30/0
4		Homo-Fe-TPY (0.1)	2 d	3/43
5		Fe-TPY-MOLs (0.02)	2 d	100/0
6		Fe-TPY-MOLs (0.2)	1 d	95/0
7		Fe-TPY-MOLs (0.2)	2 d	96/0
8		Fe-TPY-MOLs (0.2)	2 d	90/0
9[b]		Fe-TPY-MOLs (0.2)	1 d	100/0
10[c]		Fe-TPY-MOLs (0.2)	4 d	85/0

[a] Entries 1–8: Yields determined by ^{1}H NMR spectroscopy with mesitylene as the internal standard. Entries 9 and 10: Yields determined by GC-MS. [b] At 70 °C with Et_2SiH_2 as the silane. [c] At 100 °C with Ph_2SiH_2 as the silane.

3D structure. The zero or low activity of the MOF catalysts can be attributed to the limited diffusion rates of the substrates and product in the MOF channels, highlighting the advantage of MOLs over traditional MOFs as heterogeneous molecular catalysts as diffusional constraints are relieved. The MOLs were separated from the reaction by centrifugation, and reused four times without loss of activity (Figure S15). The heterogeneous nature of the catalysis was confirmed by the lack of activity of the reaction supernatant after MOL removal by centrifugation. (Figure S16).

The substrate scope was also explored (Table 1, entries 6–10). Interestingly, the MOLs gave pure anti-Markovnikov products for all of the substrates whereas the "homogeneous" counterpart Homo-Fe-TPY was selective towards the Markovnikov product and exhibited approximately 10 times lower activity (Table 1, entry 4). It is likely that Homo-Fe-TPY decomposed under the reaction conditions to afford Fe^0 nanoparticles, which act as a less effective catalyst for the hydrosilylation reaction with selectivity for the Markovnikov product. These results indicate that the MOL-immobilized Fe-TPY species can act as true molecular catalysts by preventing bimolecular disproportionation through site isolation in MOLs.

In summary, we have developed a scalable bottom-up strategy for synthesizing stable MOLs with the thinness of a single monolayer in a one-pot solvothermal reaction. We have shown that MOL catalysts significantly outperform traditional MOFs in terms of activity by removing the diffusional constraints imposed on substrates and products. This work promises to open up a new class of two-dimensional coordination materials with molecular functionalities for innovative applications.

Acknowledgements

The present research was financially supported by the National Natural Science Foundation of P.R. China (21471126), the National Thousand Talents Program of P.R. China, the 985 Program of Chemistry and Chemical Engineering disciplines of Xiamen University, and the US National Science Foundation (CHE-1464941). Additional support was provided by the Chicago MRSEC, which is funded by the NSF through grant DMR-1420709. Single-crystal diffraction studies were performed at ChemMatCARS, APS, Argonne National Laboratory (ANL), which is principally supported by the National Science Foundation (NSF/CHE-1346572). XAS analysis was performed at Beamline 9-BM, APS, ANL. Use of the APS, an Office of Science User Facility operated for the U.S. Department of Energy (DOE) Office of Science by Argonne National Laboratory, was supported by the U.S. DOE (DE-AC02-06CH11357).

Keywords: alkenes · hafnium · heterogeneous catalysis · hydrosilylation · metal–organic layers

How to cite: *Angew. Chem. Int. Ed.* **2016**, *55*, 4962–4966
Angew. Chem. **2016**, *128*, 5046–5050

[1] a) K. Manna, T. Zhang, W. Lin, *J. Am. Chem. Soc.* **2014**, *136*, 6566; b) S. H. Cho, B. Ma, S. T. Nguyen, J. T. Hupp, T. E. Albrecht-Schmitt, *Chem. Commun.* **2006**, 2563; c) S. M. Cohen, *Chem. Rev.* **2012**, *112*, 970; d) T. Haneda, M. Kawano, T. Kawamichi, M. Fujita, *J. Am. Chem. Soc.* **2008**, *130*, 1578; e) K. M. Choi, K. Na, G. A. Somorjai, O. M. Yaghi, *J. Am. Chem. Soc.* **2015**, *137*, 7810; f) D. Feng, Z.-Y. Gu, J.-R. Li, H.-L. Jiang, Z. Wei, H.-C. Zhou, *Angew. Chem. Int. Ed.* **2012**, *51*, 10307; *Angew. Chem.* **2012**, *124*, 10453; g) M. Zhao, S. Ou, C.-D. Wu, *Acc. Chem. Res.* **2014**, *47*, 1199; h) K.-K. Yee, Y.-L. Wong, M. Zha, R. Y. Adhikari, M. T. Tuominen, J. He, Z. Xu, *Chem. Commun.* **2015**, *51*, 10941; i) D. J. Xiao, E. D. Bloch, J. A. Mason, W. L. Queen, M. R. Hudson, N. Planas, J. Borycz, A. L. Dzubak, P. Verma, K. Lee, F. Bonino, V. Crocellà, J. Yano, S. Bordiga, D. G. Truhlar, L. Gagliardi, C. M. Brown, J. R. Long, *Nat. Chem.* **2014**, *6*, 590.

[2] F. Song, C. Wang, J. M. Falkowski, L. Ma, W. Lin, *J. Am. Chem. Soc.* **2010**, *132*, 15390.

[3] A. Bétard, R. A. Fischer, *Chem. Rev.* **2012**, *112*, 1055.

[4] a) K. S. Novoselov, A. K. Geim, S. V. Morozov, D. Jiang, Y. Zhang, S. V. Dubonos, I. V. Grigorieva, A. A. Firsov, *Science* **2004**, *306*, 666; b) K. F. Mak, C. Lee, J. Hone, J. Shan, T. F. Heinz, *Phys. Rev. Lett.* **2010**, *105*, 136805.

[5] a) S. Stepanow, N. Lin, D. Payer, U. Schlickum, F. Klappenberger, G. Zoppellaro, M. Ruben, H. Brune, J. V. Barth, K. Kern, *Angew. Chem. Int. Ed.* **2007**, *46*, 710; *Angew. Chem.* **2007**, *119*, 724; b) T. Lin, G. Kuang, W. Wang, N. Lin, *ACS Nano* **2014**, *8*, 8310.

[6] a) R. Dong, M. Pfeffermann, H. Liang, Z. Zheng, X. Zhu, J. Zhang, X. Feng, *Angew. Chem. Int. Ed.* **2015**, *54*, 12058; *Angew. Chem.* **2015**, *127*, 12226; b) T. Bauer, Z. Zheng, A. Renn, R. Enning, A. Stemmer, J. Sakamoto, A. D. Schlüter, *Angew. Chem. Int. Ed.* **2011**, *50*, 7879; *Angew. Chem.* **2011**, *123*, 8025; c) R. Sakamoto, K. Hoshiko, Q. Liu, T. Yagi, T. Nagayama, S. Kusaka,

M. Tsuchiya, Y. Kitagawa, W. Y. Wong, H. Nishihara, *Nat. Commun.* **2015**, *6*, 6713.

[7] a) Y. Peng, Y. Li, Y. Ban, H. Jin, W. Jiao, X. Liu, W. Yang, *Science* **2014**, *346*, 1356; b) P. Z. Li, Y. Maeda, Q. Xu, *Chem. Commun.* **2011**, *47*, 8436; c) P. Amo-Ochoa, L. Welte, R. González-Prieto, P. J. Sanz Miguel, C. J. Gómez-García, E. Mateo-Martí, S. Delgado, J. Gómez-Herrero, F. Zamora, *Chem. Commun.* **2010**, *46*, 3262.

[8] a) M. Zhao, Y. Wang, Q. Ma, Y. Huang, X. Zhang, J. Ping, Z. Zhang, Q. Lu, Y. Yu, H. Xu, Y. Zhao, H. Zhang, *Adv. Mater.* **2015**, *27*, 7372; b) S. C. Junggeburth, L. Diehl, S. Werner, V. Duppel, W. Sigle, B. V. Lotsch, *J. Am. Chem. Soc.* **2013**, *135*, 6157.

[9] H. X. Lin, Z. C. Lei, Z. Y. Jiang, C. P. Hou, D. Y. Liu, M. M. Xu, Z. Q. Tian, Z. X. Xie, *J. Am. Chem. Soc.* **2013**, *135*, 9311.

[10] a) J. H. Cavka, S. Jakobsen, U. Olsbye, N. Guillou, C. Lamberti, S. Bordiga, K. P. Lillerud, *J. Am. Chem. Soc.* **2008**, *130*, 13850; b) R. Wang, Z. Wang, Y. Xu, F. Dai, L. Zhang, D. Sun, *Inorg. Chem.* **2014**, *53*, 7086; c) F. Vermoortele, B. Bueken, G. Le Bars, B. Van de Voorde, M. Vandichel, K. Houthoofd, A. Vimont, M. Daturi, M. Waroquier, V. Van Speybroeck, C. Kirschhock, D. E. De Vos, *J. Am. Chem. Soc.* **2013**, *135*, 11465.

[11] S. Stankovich, D. A. Dikin, R. D. Piner, K. A. Kohlhaas, A. Kleinhammes, Y. Jia, Y. Wu, S. T. Nguyen, R. S. Ruoff, *Carbon* **2007**, *45*, 1558.

[12] a) L. Zhu, D. Zhang, M. Xue, H. Li, S. Qiu, *CrystEngComm* **2013**, *15*, 9356; b) C. Wiktor, S. Turner, D. Zacher, R. A. Fischer, G. V. Tendeloo, *Microporous Mesoporous Mater.* **2012**, *162*, 131; c) M. Díaz-García, Á. Mayoral, I. Díaz, M. Sánchez-Sánchez, *Cryst. Growth Des.* **2014**, *14*, 2479.

[13] CCDC 1444732 and 1444733 contain the supplementary crystallographic data for this paper. These data can be obtained free of charge from The Cambridge Crystallographic Data Centre.

[14] A. M. Tondreau, C. C. H. Atienza, K. J. Weller, S. A. Nye, K. M. Lewis, J. G. P. Delis, P. J. Chirik, *Science* **2012**, *335*, 567.

Received: December 31, 2015
Revised: February 9, 2016
Published online: March 8, 2016

